

## The Operational CMC–MRB Global Environmental Multiscale (GEM) Model. Part II: Results

JEAN CÔTÉ

*Meteorological Research Branch, Atmospheric Environment Service, Dorval, Quebec, Canada*

JEAN-GUY DESMARAIS

*Canadian Meteorological Centre, Atmospheric Environment Service, Dorval, Quebec, Canada*

SYLVIE GRAVEL

*Meteorological Research Branch, Atmospheric Environment Service, Dorval, Quebec, Canada*

ANDRÉ MÉTHOT AND ALAIN PATOINE

*Canadian Meteorological Centre, Atmospheric Environment Service, Dorval, Quebec, Canada*

MICHEL ROCH AND ANDREW STANIFORTH

*Meteorological Research Branch, Atmospheric Environment Service, Dorval, Quebec, Canada*

(Manuscript received 31 March 1997, in final form 3 October 1997)

### ABSTRACT

An integrated forecasting and data assimilation system has been and is continuing to be developed by the Meteorological Research Branch (MRB) in partnership with the Canadian Meteorological Centre (CMC) of Environment Canada. Part II of this two-part paper presents the objective and subjective evaluations of the intercomparison process that led to the operational implementation of the new Global Environmental Multiscale model. The results of a “proof of concept” experiment and those of a meso- $\gamma$ -scale simulation further demonstrate the validity and versatility of this model.

### 1. Introduction

In Part I (Côté et al. 1998) of this two-part paper, the staged and ongoing long-term development of a comprehensive and fully integrated global atmospheric environmental forecasting and simulation system is motivated and described. This system is being built around the GEM (Global Environmental Multiscale) model, a global variable-resolution model that is designed such that it can be configured to forecast and simulate the atmosphere over a broad range of scales, from the global scale down to the meso- $\gamma$  scale.

The principal goals of Part II are to present the following:

- An overview of the medium-range uniform-resolution performance of the GEM model by comparing it to

that of a state-of-the-art operational global spectral model.

- An assessment of the global variable-resolution strategy for continental-scale regions by comparing the forecast obtained using a variable-resolution mesh with that of a high- and uniform-resolution control integration.
- Objective and subjective evaluations of the almost three-month-long twice-daily preimplementation comparisons with the formerly operational Regional Finite Element (RFE) model that led to its operational implementation on 24 February 1997 for regional weather forecasting at the Canadian Meteorological Centre (CMC).
- An assessment of the numerical feasibility of using a global variable resolution strategy for simulating events at the meso- $\gamma$  scale.

### 2. Medium-range uniform-resolution results

Since October 1996 and with only relatively minor changes, a medium-range configuration of the GEM

---

*Corresponding author address:* Dr. Jean Côté, Recherche en Prévision Numérique, 2121 Route Transcanadienne, Dorval, PQ H9P 1J3, Canada.  
E-mail: jean.cote@ec.gc.ca

TABLE 1. Principal attributes of the spectral (SEF) and global uniform-resolution GEM model configurations for the comparisons.

	SEF model	GEM model
Horizontal mesh (resolution)	400 × 200 Gaussian grid (T199 ~ 0.9°)	400 × 200 uniform grid (0.9°)
Levels	21 sigma	28 hybrid
Spatial discretization	2D spectral + 1D finite element	3D finite element
Time discretization	3-time-level, semi-implicit/semi-Lagrangian	2-time-level, implicit/semi-Lagrangian
Time step	30 min	40 min
Horizontal diffusion coefficient	$\nabla^2$ $\nu_{\text{average of 1st 3 days}} = 5 \times 10^4 \text{ m}^2 \text{ s}^{-1}$ $\nu = 2 \times 10^4 \text{ m}^2 \text{ s}^{-1}$ at $t = 0$ , linearly increasing to $\nu = 10^5 \text{ m}^2 \text{ s}^{-1}$ at $t = 4$ days	$\nabla^2$ $\nu = 4.8 \times 10^4 \text{ m}^2 \text{ s}^{-1}$
Stratospheric sponge	Yes	No
Physics	Mailhot et al. (1995)	Mailhot et al. (1997)
Initial conditions	Analyzed directly on the 400 × 200 Gaussian grid of the global data assimilation cycle	Horizontally and vertically interpolated from the 400 × 200 Gaussian grid of the global data assimilation cycle
Dynamic balancing	Adiabatic normal mode	Diabatic digital filter

model has been systematically run once per day to both: (a) evaluate and validate the model as a replacement of the operational SEF model (Ritchie and Beaudoin 1994), and (b) accumulate model forecast statistics to specify the background error covariance matrices needed in variational data assimilation (e.g., Rabier et al. 1998). The configuration (see Table 1) was chosen to be quite similar to that of the currently operational SEF

model to facilitate forecast comparisons, but with two significant exceptions. These are the number of levels (28 for the GEM model vs 21 for the SEF model) and their placement (see Fig. 1 for a schematic representation of the GEM model levels), and the set of physical parameterizations [the most recent one of Mailhot et al. (1997), as in the operational regional configuration, versus the older one of Mailhot et al. (1995)]. The justification for these two exceptions is that we consider it desirable, to the extent reasonably possible, to initially configure the operational medium-range forecast model to have (a) the same number and placement of vertical levels as the operational short-range regional model, and (b) the same set of parameterizations.

This configuration can be expected to confer an advantage to the GEM model in any comparison against the currently operational SEF model, since the GEM model thereby has higher vertical resolution and a more evolved set of physical parameterizations. However for the comparisons presented here, against this advantage must be weighed the disadvantage that the GEM model uses degraded initial conditions due to the horizontal and vertical interpolation of a 16-level isobaric analysis (see Fig. 1 for the placement of these isobaric levels). The effect of the horizontal interpolation is negligible because the two meshes (Gaussian vs uniform latitude-longitude) are almost identical due to the fact that a Gaussian grid at high resolution asymptotes toward uniform resolution. The effect of vertical interpolation of the analysis is more serious and leads at initial time to a degraded definition of the planetary boundary layer which nevertheless typically reestablishes itself after a couple of hours, a reduction in jet intensity, and a longer precipitation spinup time. These weaknesses will be ad-

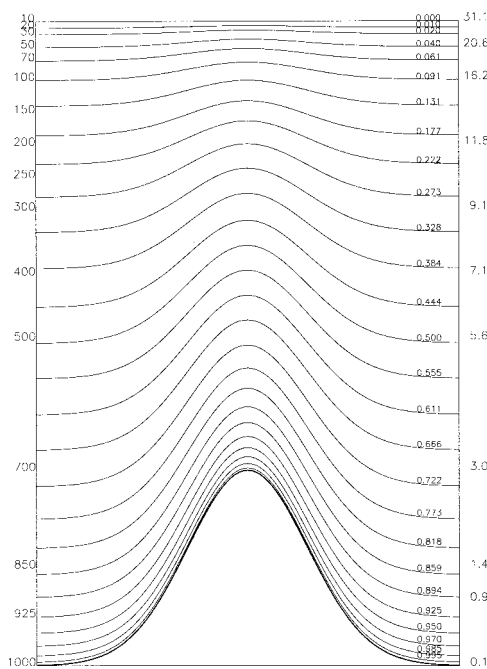


FIG. 1. Vertical mesh over an idealized mountain for the GEM model with 28 levels.

dressed when the operational uniform-resolution 3D variational data assimilation system (3DVAR) is modified to be driven by the GEM model and to produce analyses directly on the GEM model's 3D grid. Work to do this is under way and consists of running the previously described 3DVAR spinup system (see section 5 of Part I) with uniform resolution and adapting it for use in perpetual standalone mode. In particular this involves ensuring that there is no climate drift in the GEM model, something that is relatively unimportant when the system is run in spinup mode, because it is effectively restarted every 12 h from an analysis provided by an independent system with its own hopefully realistic climate. When the GEM-driven uniform-resolution 3DVAR data assimilation system is validated, the CMC plans to use it to operationally replace the present SEF-based medium-range data assimilation and forecast system.

No changes have been made to either the medium-range configuration of the GEM model or the SEF model since the end of winter 1997. At the time of writing, verification statistics are available for all 92 cases of the three-month spring period 21 March–20 June 1997. The forecasts from the two models have been verified at six standard levels (100, 250, 500, 700, 850, and 1000 hPa) against all available radiosonde soundings of a WMO standard set (approximately 425 per verification time) over the globe. The resulting scores, averaged over all cases, are displayed in Fig. 2 for the forecasts to 6 days.

The results show that on average the GEM model performs somewhat better than the operational SEF model. The GEM model has a smaller tropospheric height bias, a significantly smaller wind bias, and a smaller rms temperature error at most levels (all three plausibly due to better vertical resolution, the use of a hybrid coordinate, and the absence of an overly strong stratospheric sponge. Further, the model has smaller tropospheric temperature (except at 1000 hPa) and moisture biases (plausibly attributable to the more recent physical parameterization package of the GEM model). On the other side of the ledger however, it has a larger rms moisture error above the planetary boundary layer, possibly attributable to differences in the physical parameterization packages, and larger stratospheric height and temperature biases, possibly attributable to the absence of a stratospheric sponge in the GEM model.

### 3. Assessing the strategy for continental-scale regions

#### a. Methodology

A preliminary assessment of the global variable-mesh strategy for continental-scale regions was made in Côté et al. (1997) by comparing uniform- and variable-resolution 48-h integrations started from the same initial data, using the methodology introduced in Côté et al. (1993) for the validation of a shallow-water prototype.

All of the Côté et al. (1997) integrations were performed using the dry primitive equations in the absence of topography and also in the absence of heat and momentum fluxes. These experiments were then repeated in Staniforth (1997) but at higher ( $0.8^\circ$  vs  $1.2^\circ$ ) resolution. In all these studies it was concluded that the 48-h variable-resolution forecast over the uniform-resolution continental window well reproduces, but at a fraction of the cost, that obtained using the same uniform resolution everywhere.

The same validation methodology is adopted here. However the GEM model now includes topography and all the physical parameterizations (Mailhot et al. 1997) used operationally for regional forecasting, and the experiments are performed at substantially higher ( $0.36^\circ$ ) resolution. Ideally they should be run at the  $0.33^\circ$  resolution of the uniform-resolution window of the operational regional mesh displayed in Fig. 1 of Côté et al. (1998). Unfortunately computer memory limitations do not permit running the uniform-resolution control forecasts at quite such a high resolution at the present time. The experimental methodology is now described in more detail.

Three 48-h integrations are made starting from the same initial data, the CMC 16-level isobaric analysis valid at 1200 UTC 14 November 95. This relatively low-resolution analysis does not provide the model with a well-defined planetary boundary layer at initial time, but it is one of a series of standard cases used by the CMC to validate regional models before operational implementation, and the strong flow over the eastern Pacific, upstream of North America, is of particular interest here. A digital filtering technique based on that described in Fillion et al. (1995) is employed in all experiments to put the fields in dynamic balance, and all integrations were performed with the 28 vertical levels shown schematically in Fig. 1, a time step of 22.5 min, and a Laplacian diffusion with a coefficient of  $2 \times 10^4 \text{ m}^2 \text{ s}^{-1}$ . The three experimental configurations are summarized in Table 2. The purpose of the two uniform-resolution experiments is to validate a uniform-resolution ground truth (experiment B) against which the variable-resolution forecast of experiment C can be compared and evaluated. Both uniform-resolution experiments were performed at  $0.36^\circ$  resolution (in both longitude and latitude), using a mesh with the poles of the coordinate system either coincident with respect to the geographical ones (experiment A), or rotated as in Fig. 3a (experiment B).

The variable-resolution experiment C was performed on the mesh depicted in Fig. 3b, where the poles of the coordinate system are rotated with respect to the geographical ones. Its purpose is to demonstrate the thesis that the variable-resolution forecast over the  $0.36^\circ$  uniform-resolution continental window well reproduces, but at a fraction of the cost, that obtained using  $0.36^\circ$  uniform resolution everywhere. The resolution of the mesh is uniform ( $0.36^\circ$ ) over a  $59.04^\circ \times 76.68^\circ$  window

## GEM (solid) vs SEF (dashed)

Bias and r.m.s. errors against global radiosonde network  
average of 92 forecasts: 21 March to 20 June 1997

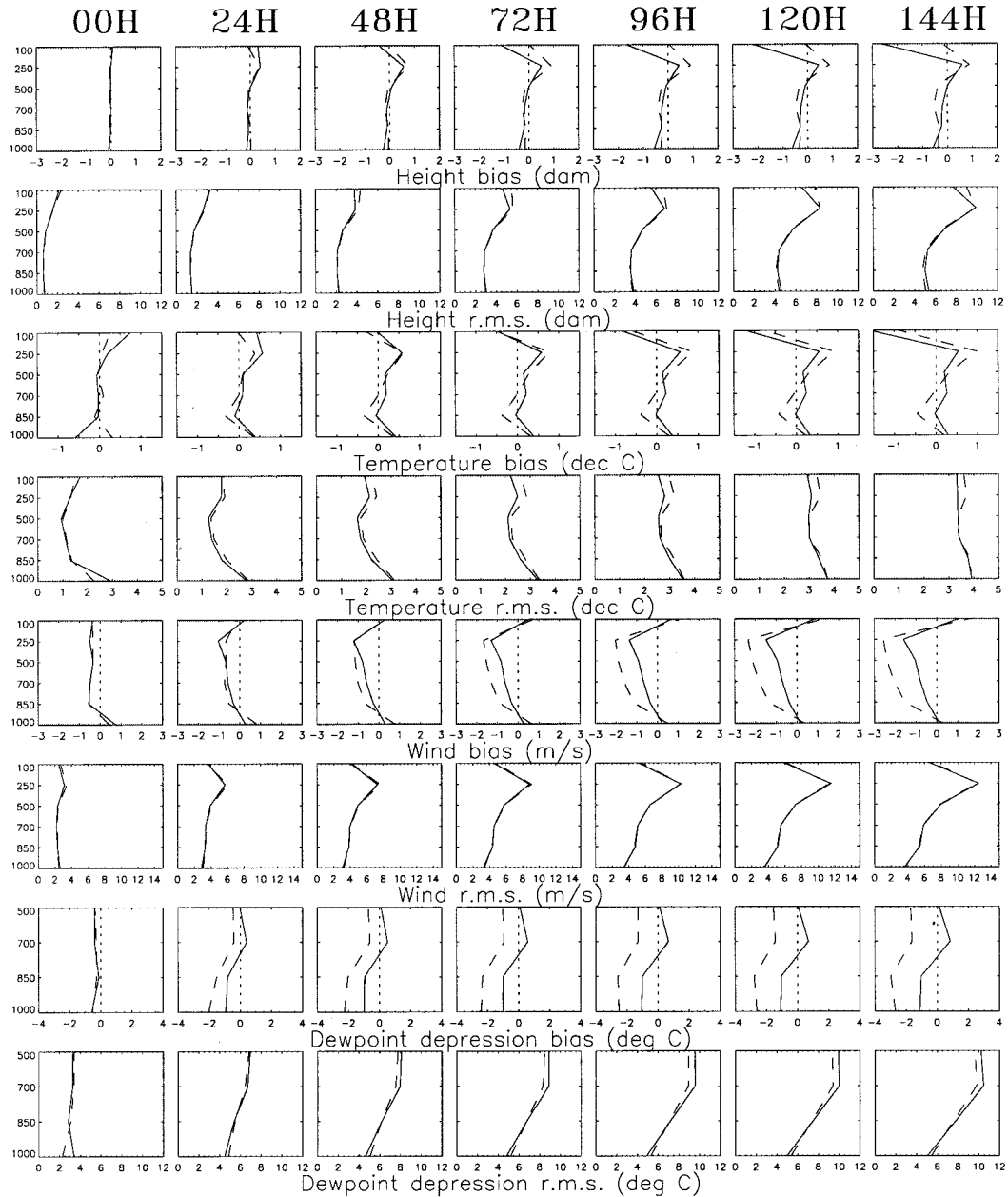


FIG. 2. Bias and rms forecast errors of the SEF (dashed) and GEM (solid) models, as a function of time (going from left to right), and as measured against radiosonde soundings of a global network (about 425 per verification time). The errors for height (dam), temperature (K), wind ( $\text{m s}^{-1}$ ), and dewpoint depression (K) are averaged over 92 cases from the period 21 March–20 June 1997. The ordinate for each panel is pressure (hPa).

centered on a point of the equator of a rotated coordinate system located at  $58^{\circ}\text{N}$ ,  $100^{\circ}\text{W}$  in geographical coordinates. Uniform resolution again refers to uniform spacing in latitude and longitude: however the mesh points of the window are also almost uniformly spaced

over the sphere with a mesh length that varies between approximately 31 and 40 km. Outside the window, the resolution degrades smoothly away in each direction with each successive mesh length being approximately 10% larger than its predecessor. The gradual transition

TABLE 2. Experimental configurations.

Expt.	Rotated coordinate system?	Mesh dimensions	Uniform/variable	Resolution
A	No	1000 × 500	Uniform	0.36° everywhere
B	Yes, centered on 58°N, 100°W	1000 × 500	Uniform	0.36° everywhere
C	Yes, centered on 58°N, 100°W	240 × 268	Variable	0.36° on 59.04° × 76.68° window

from fine to coarse resolution allows an adequate representation of the flow features in the vicinity of the uniform window that are subsequently advected over the domain of interest during the course of the short-term integration. Too large an expansion factor—25% for example—would lead to larger forecast errors over the area of interest. The cost of the uniform-resolution experiments is about seven times that of the variable-resolution experiment, a little less than the ratio of the number of grid points.

#### b. Uniform-resolution experiments

The 500-hPa height and mean sea level pressure (MSLP) fields of the initial analysis used for the experiments are shown in Fig. 4. The global rms forecast differences (computed after interpolating the forecast of experiment A to the rotated mesh of experiment B) of the resulting 2-day forecasts of these fields for experiments A and B (i.e., using uniform 0.36° resolution on the unrotated and rotated meshes) are 4.44 m and 0.58 hPa, respectively. This shows that the effect of rotating the mesh by 83.37° along a meridian while keeping its resolution uniform is acceptably small. The 2-day forecast for experiment B (i.e., uniform resolution everywhere in the rotated coordinate system) is shown in Fig. 5.

#### c. Variable-resolution experiment

Experiment B is considered to be the ground truth for the purpose of validating the 48-h forecast of the variable-resolution integration (experiment C). Note that the meshes of both integrations are identical over the uniform resolution window of Fig. 3b. The 2-day variable-resolution forecast is shown in Fig. 6 and may be compared to that of the control (Fig. 5). The two forecasts (experiment B vs C) are quite close over the uniform-resolution area of interest (defined by the curvilinear rectangle of Fig. 6a). This confirms the thesis that the variable-resolution forecast over the 0.36° uniform-resolution continental window well reproduces, but at a fraction of the cost, that obtained using 0.36° uniform resolution everywhere. However, they are significantly different over areas of low resolution, as indeed they should be. The differences (see Fig. 7) between the forecasts of experiments B and C increase as a function of distance from the boundary of the uniform-resolution window, consistent with theory. Quantifying

this, the global rms differences between the forecasts of experiments B and C are 42.3 m and 3.85 hPa for the 500-hPa height and MSLP fields respectively, whereas they are only 5.24 m and 0.48 hPa over the curvilinear rectangle, where the mesh points of the two grids are coincident. These latter differences are of the same order as those between experiments A and B computed over the same curvilinear rectangle (3.85 m and 0.66 hPa, respectively), which both use the same uniform-resolution meshes but rotated with respect to one another.

#### d. Comparison of forecasts against analyses

Experiments A–C are designed to test the thesis that a 48-h control forecast obtained using uniform resolution everywhere can be well reproduced over the uniform-resolution window of a variable-resolution integration, but at a fraction of the cost. This is a numerical sensitivity test. Consequently it does not measure the actual quality of any of the forecasts, only their closeness to one another. To examine the quality of the forecasts displayed in Figs. 5 and 6, they can be compared with the corresponding verifying analyses shown in Fig. 8. It is seen that forecast quality is generally quite good, albeit with room for improvement, and this is quantified in Table 3 over the 59.04° × 76.68° window of interest. Note that the use of a rotated horizontally varying mesh degrades only marginally (~5%) the accuracy of the forecast with respect to the uniform-resolution control one of experiment A. Note also that for all experiments, the MSLP errors in mountainous regions are unreliable due to the uncertainty in MSLP-reduction algorithms.

#### e. Comparison of forecasts against those of the RFE model

It is also of interest to compare the quality of the variable-resolution forecasts (Fig. 6) of experiment C with the corresponding ones displayed in Fig. 9 for the RFE model. A priori, the two models are expected to give similar results since they have approximately the same uniform resolution focused on approximately the same geographical area, they have the same number of vertical levels, and they use the identical set of physical parameterizations.

The forecasts of the GEM and RFE models are strikingly similar and they agree well with the corresponding objective analysis, albeit with some common failings.



FIG. 3a. The uniform  $0.36^\circ$  resolution  $1000 \times 500$  mesh used for experiment B.

For the geopotential field, both models underestimate the northwestward extent of the westcoast ridge, as well as the speed and intensity of the short-wave trough that is superimposed on the large-scale ridge over the western part of Canada. They also overestimate the intensity of the ridge off the Canadian east coast (cf. Figs. 6a, 9a, and 8a). For the MSLP pressure field, both models (Fig. 6b, 9b) exhibit some errors when compared to the analysis (Fig. 8b), especially over the western part of the domain of interest, the Rocky Mountains, and Greenland. For the latter two locations, the previously mentioned use (see section 3d) of different MSLP-reduction algorithms by the forecast models and in the analysis cycle may partially explain the differences.

The main differences between the 500-hPa geopotential height forecasts of the GEM and the RFE models are (a) the low located just east of James Bay, which is 2 dam deeper in the GEM model's forecast; and (b) the 532-dam closed low east of the southern tip of Greenland. In both cases the GEM model's forecast is closer to the verifying analysis, and this contributes to the marginally lower rms height errors given in Table 3. The associated MSLP features also manifest a similar behavior, with the GEM model giving a depth and position closer to the analysis for both systems.

#### 4. Preimplementation comparisons: Objective evaluation

From 1 December 1996 until its operational implementation on 24 February 1997, the new variable-resolution GEM model was integrated twice daily by the CMC in a preimplementation run. It was configured to be quite close to that of the RFE model to facilitate its validation for operational forecasting: forecasts from the two models were compared against one another, and also against analyses and observations. The principal attributes of the two model configurations are summarized in Table 4. Both models are configured to have almost the same resolution over a North American window of almost the same size, the same number of vertical levels with almost the same placement, and identical physical parameterization packages (Mailhot et al. 1997).

The most important difference between the two setups is probably that of the initial conditions. The RFE model was initialized from an analysis resulting from a 12-h data assimilation spinup cycle (Chouinard et al. 1994). At the time of the evaluation, the development of an analogous spinup cycle driven by the GEM model was insufficiently advanced to be used. To obtain its initial state, the GEM model therefore relied on an analysis



FIG. 3b. A variable-resolution  $240 \times 268$  mesh having a  $59.04^\circ \times 76.68^\circ$  window of uniform  $0.36^\circ$  resolution, centered on  $58^\circ\text{N}$ ,  $100^\circ\text{W}$ , and used for experiment C.

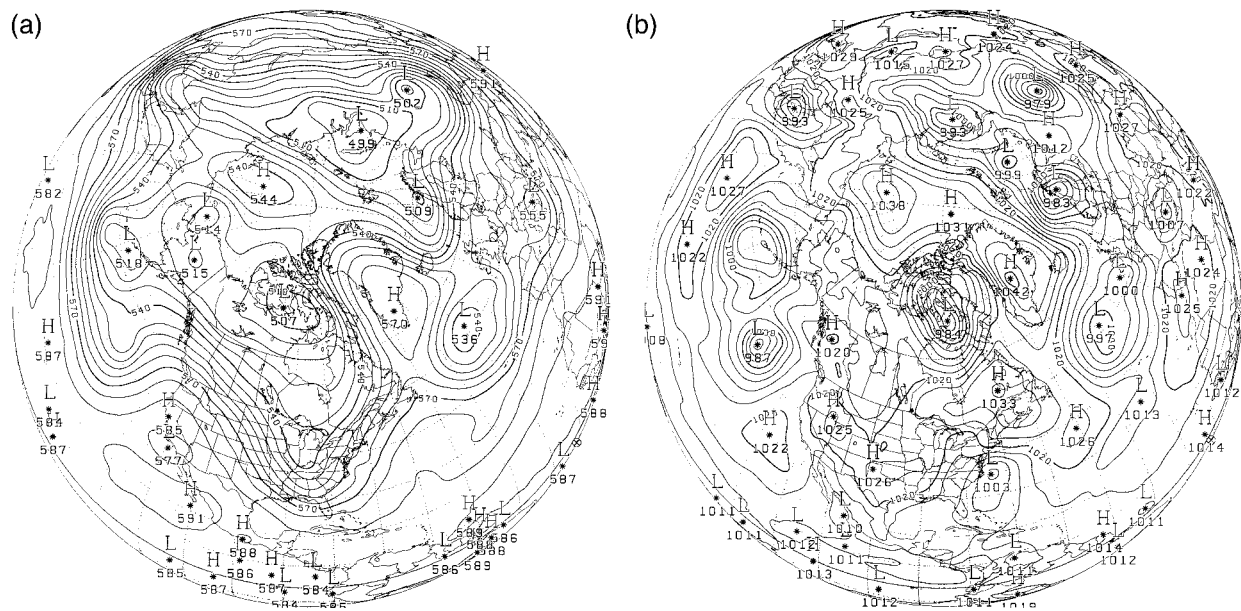


FIG. 4. (a) Initial geopotential height (dam) at 500 hPa on an orthographic projection; contour interval is 6 dam. (b) Initial MSLP (hPa) on an orthographic projection; contour interval is 4 hPa.

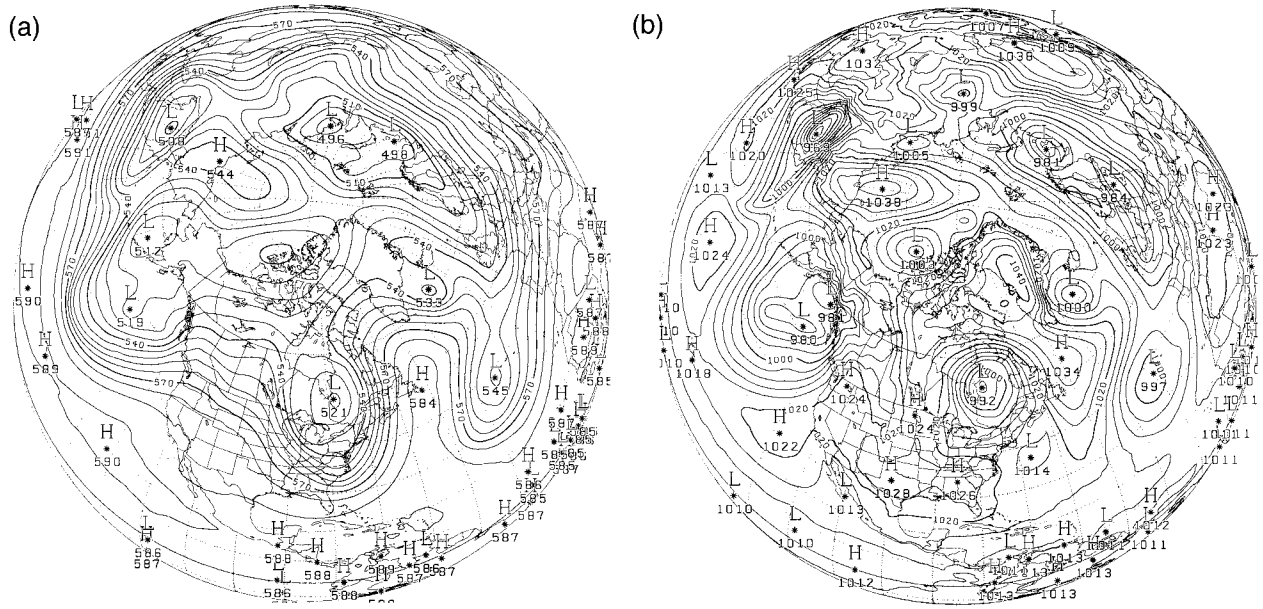


FIG. 5. (a) Same as in Fig. 4a, but at 48 h for experiment B. (b) Same as in Fig. 4b, but at 48 h for experiment B.

provided by a global data assimilation cycle (Mitchell et al. 1996) driven by CMC's spectral model. This 16-pressure-level analysis (see Fig. 1 for level distribution) is defined on a  $400 \times 200$  Gaussian grid, and it was vertically and horizontally interpolated to the GEM model's variable-resolution mesh. It was assumed that if the GEM model performs well using this analysis as initial conditions, then it will also perform well with an analysis provided by its own 3DVAR data assimilation spinup cycle, once this model is sufficiently developed

and validated for operational implementation [for additional discussion, see section 5 of Côté et al. (1998)]. Both assimilation cycles, the regional one (driven by the RFE model), and the global one (driven by the spectral model) that provides the GEM model with its initial conditions, used the same data cutoff times of 0150 and 1350 UTC, respectively, for the 0000 and 1200 UTC analyses, and consequently used identical observational datasets.

Despite the differences in initial conditions and some

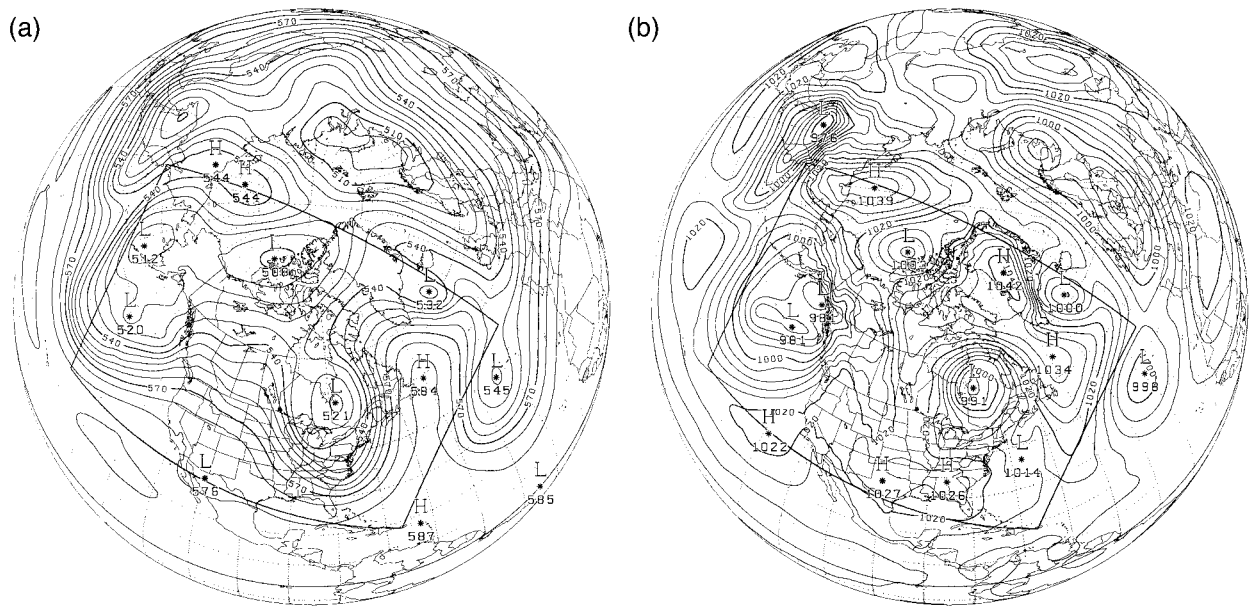


FIG. 6. (a) Same as in Fig. 4a, but at 48 h for experiment C. (b) Same as in Fig. 4b, but at 48 h for experiment C.

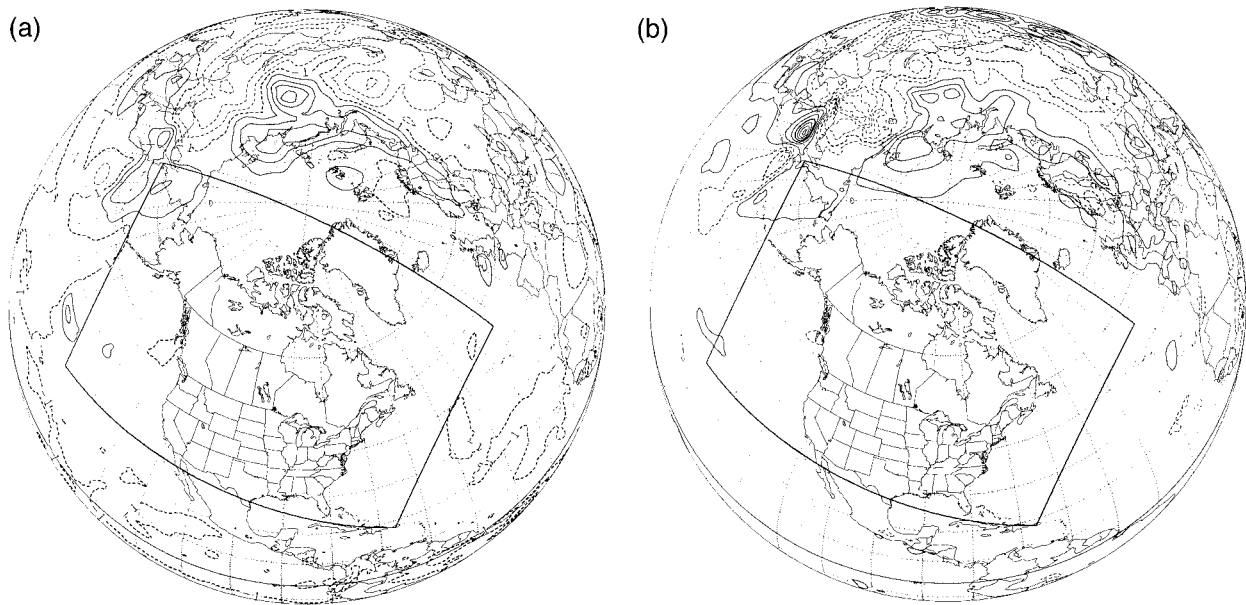


FIG. 7. Difference between 48-h forecasts of experiments B and C on an orthographic projection for (a) 500-hPa geopotential height; contours are  $\pm 10$ ,  $\pm 30$ ,  $\pm 50$  m, etc. (b) MSLP: contours are  $\pm 1$ ,  $\pm 3$ ,  $\pm 5$  hPa, etc.

differences in numerical techniques, a priori it was expected that given the chosen configurations (Table 4), the two models should perform similarly. Quantitative and qualitative evaluations of these comparative forecasting experiments are given in this section and the next, respectively.

*a. Bias and rmse statistics*

Verification statistics are available for 163 48-h forecasts and are displayed in Fig. 10. The forecasts from

the two models are verified against all radiosonde soundings over the uniform-resolution North American subdomain. This verification has the virtue of providing a model-independent measure of the truth at the following standard isobaric levels: 100, 250, 500, 700, 850, 925, and 1000 hPa. There are approximately 120 soundings available per verification time and a typical station distribution is shown in Fig. 11.

The results indicate that the overall performance of the two models is, as expected, very similar. The rms

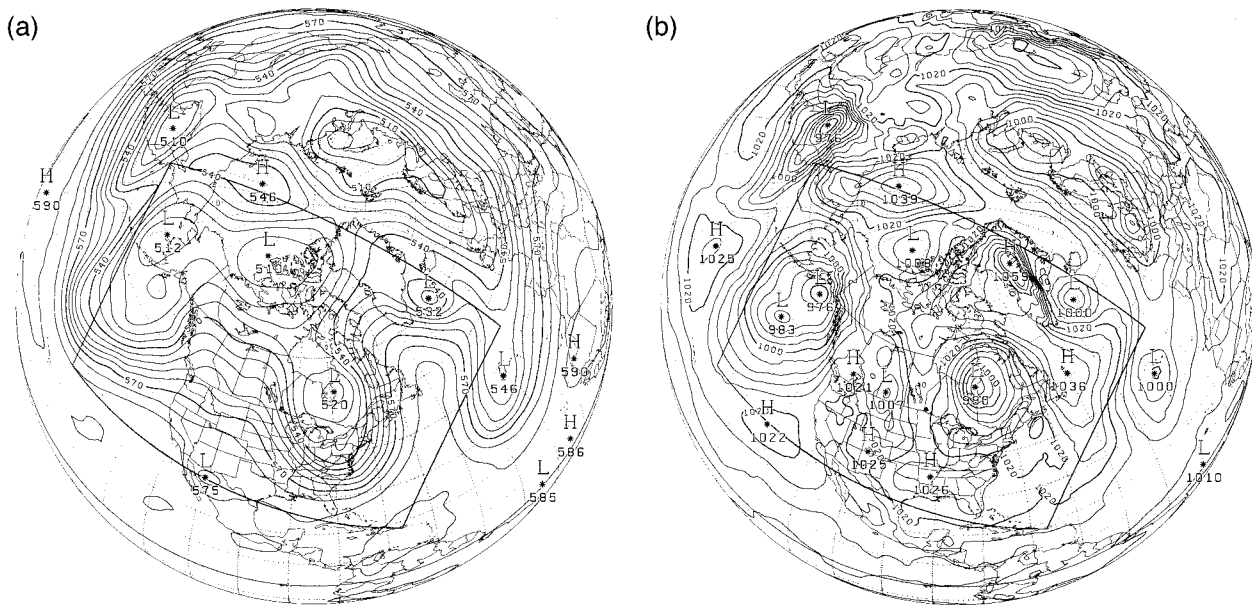


FIG. 8. (a) Same as in Fig. 4a, but for 48-h verifying analysis. (b) Same as in Fig. 4b, but for 48-h verifying analysis.

TABLE 3. Root-mean-square errors, over the  $59.04^{\circ} \times 76.68^{\circ}$  uniform-resolution window of Fig. 3b, of 48-h forecasts of 500-hPa height and msl pressure for experiments A, B, C, and the RFE model, where the analysis is taken as truth.

Forecast	500-hPa height (m)	MSLP (hPa)
Expt. A (uniform-resolution unrotated mesh)	22.10	3.11
Expt. B (uniform-resolution rotated mesh)	22.35	3.20
Expt. C (variable-resolution rotated mesh)	22.86	3.27
RFE model	23.29	3.44

height and temperature errors of the two models are comparable throughout most of the integration period. The GEM model however has a somewhat stronger negative height bias, a slightly stronger positive temperature bias in the middle troposphere, and, toward the end of the integration period, a somewhat smaller rms height error. The rms wind errors are virtually identical for both models, but the GEM model has a systematically smaller wind bias. The stronger wind bias of the RFE model might be due to the imposition of an equatorial wall and a subsequent spurious adjustment of the wind field. The rms dewpoint-depression errors are also very similar for both models, with a slight advantage to the RFE model, but the bias indicates that the GEM model is systematically too dry, particularly at longer time ranges.

Note, however, that the moisture variable carried by both models is specific humidity. Dewpoint depression and relative humidity are obtained by postprocessing

the specific humidity using appropriate thermodynamic relations that involve the temperature field. Because the GEM model's atmosphere is slightly warmer in the middle troposphere than that of the RFE model, the observed differences in the dewpoint-depression biases of the two models may be partially due to their difference in temperature bias. Also, care must be exercised with dewpoint-depression forecasts since a given difference is far more significant when it occurs for low values of dewpoint depression (i.e., for moist areas) than for high ones (i.e., for dry areas).

Some of the performance deficiencies of the GEM model may be plausibly linked to the initial conditions used in the comparison. The RFE model benefits from its use of a spinup analysis (Chouinard et al. 1994) made at high resolution on its own model grid, whereas the initial conditions for the GEM model were obtained from a horizontal and vertical interpolation of a lower- and uniform-resolution global analysis. The lack of a spinup cycle can be expected to result at initial time in both a less-detailed planetary boundary layer and a tropospheric jet of reduced intensity, and also a longer time for the precipitation rate to attain realistic values at the beginning of the forecast period. Subsequent results (to be shown elsewhere by others) obtained using a GEM-driven 3DVAR data assimilation spinup cycle (a brief summary of this system is given in section 5 of Part I) indicate that the precipitation rate early in the forecast period is dramatically improved.

Several attributes of the GEM model probably help compensate for the two a priori disadvantages of the poor initial conditions, and the use of a physical parameterization package developed and tuned for optimum

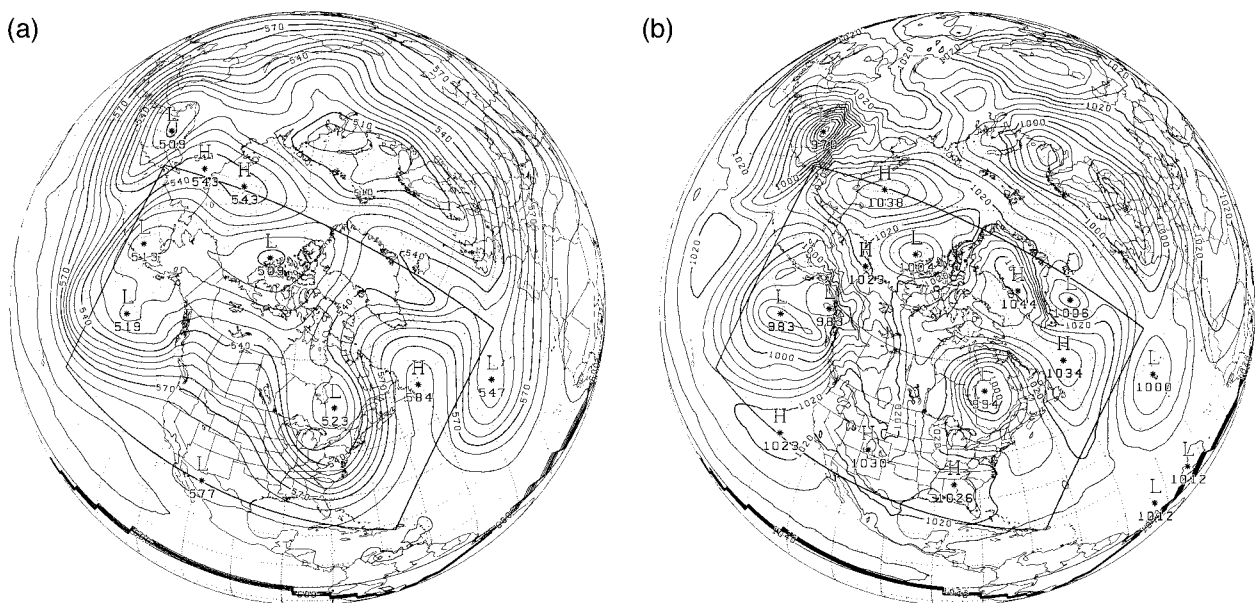


FIG. 9. (a) Same as in Fig. 4a, but for 48-h RFE forecast. (b) Same as in Fig. 4b, but for 48-h RFE forecast.

TABLE 4. Principal attributes of the RFE and GEM model configurations.

	RFE model	GEM model
Horizontal mesh	305 × 255 hemispheric	289 × 255 global
High-resolution North American window	245 × 190	235 × 180
Resolution over high-resolution window	35 km on a polar-stereographic projection (~38–25 km on globe)	0.33° on globe (~37–29 km on globe)
Levels	28 sigma	28 hybrid
Spatial discretization	3D finite element	3D finite element
Time discretization	Three-time-level, semi-implicit/semi-Lagrangian	Two-time-level, implicit/semi-Lagrangian
Time step	600 s	1350 s
Horizontal diffusion coefficient	$\nabla^2$ $\nu = 2 \times 10^4 \text{ m}^2 \text{ s}^{-1}$ (applied twice)	$\nabla^2$ $\nu = 2 \times 10^4 \text{ m}^2 \text{ s}^{-1}$ (applied once)
Stratospheric momentum sponge	Yes	No
Physics	As in Mailhot et al. (1997)	As in Mailhot et al. (1997)
Initial conditions	Analyzed directly on the RFE mesh using a 12-h regional spinup data assimilation cycle	Horizontally and vertically interpolated from the 400 × 200 Gaussian grid of the global data assimilation cycle
Dynamic balancing	Adiabatic implicit normal mode	Diabatic digital filter

performance for the RFE model and not for the GEM model. First, the GEM model is of global extent, and therefore does not suffer from the presence of the artificial wall of the RFE model in the vicinity of the equator. Second, it is somewhat more active than the RFE model. This is due to both the lower effective horizontal diffusion of the GEM model, and to the absence of the overly strong sponge layer present near the top of the RFE model. Also, the use of a hybrid vertical coordinate in the GEM model, rather than the sigma coordinate of the RFE model, has the virtue of providing coordinate surfaces that are less influenced at upper levels by the horizontal detail of the underlying topography. Fourth, the GEM model has a somewhat improved resolution over the Pacific, upstream of North America, when compared to that of the RFE model.

*b. Statistically postprocessed forecasts*

Statistically postprocessed forecasts are derived using a perfect-prog approach, with most of the predictors used in the regression equation being directly related to the mass fields of the model. The equations were elaborated using 22 years of analysis, and are described in detail in Verret (1987). The performance of the statistical forecasts are measured in terms of explained variance using the following expression:

$$\text{explained variance} = 1 - \frac{\sum_k (P_k - O_k)^2}{\sum_k (C_k - O_k)^2},$$

where  $P_k$ ,  $O_k$ , and  $C_k$  are, respectively, the statistical forecast, observation, and climatology for each station. Table 5 summarizes the results for both temperature and precipitation forecasts for the period from 1 December

1996 until 5 February 1997, when the CMC terminated this component of the comparison. As the predictor used for the 0000 and 1200 UTC forecasts are different, the scores for both are given. The 6-h postprocessed temperature forecasts of both models are very similar, with differences of less than 1%. However the 12-h postprocessed probability-of-precipitation forecasts based on the GEM model systematically show slightly better skill than the equivalent ones based on the RFE model: approximately two percentage points more variance is explained by the forecasts based on the GEM model. A case-by-case evaluation has also shown that the statistically postprocessed forecasts based on the GEM model are more discriminating inasmuch as they are more likely to predict values at the extremes of the predictand spectrum.

**5. Preimplementation comparisons: Subjective evaluation**

While it is very important to evaluate a model's performance using objective measures, such an evaluation is in practice incomplete since no set of sufficiently complete objective measures is known. A synoptic analysis—often of a single realization—is therefore commonly used as a complementary evaluation of a model's behavior. A subjective evaluation, resulting from a careful daily examination and comparison by the CMC operational meteorologists of forecasts during the preimplementation period and conducted independently of the developers of the GEM model, is presented below. This type of assessment is essential to ascertain the day-to-day performance of a new model for the prediction of those features that are significant for real-time daily weather forecasting activities. Attention was focused

### GEM (solid) vs RFE (dashed)

Bias and r.m.s. errors against N. American radiosonde soundings  
 Average for 163 forecasts: December 1996, January and February 1997

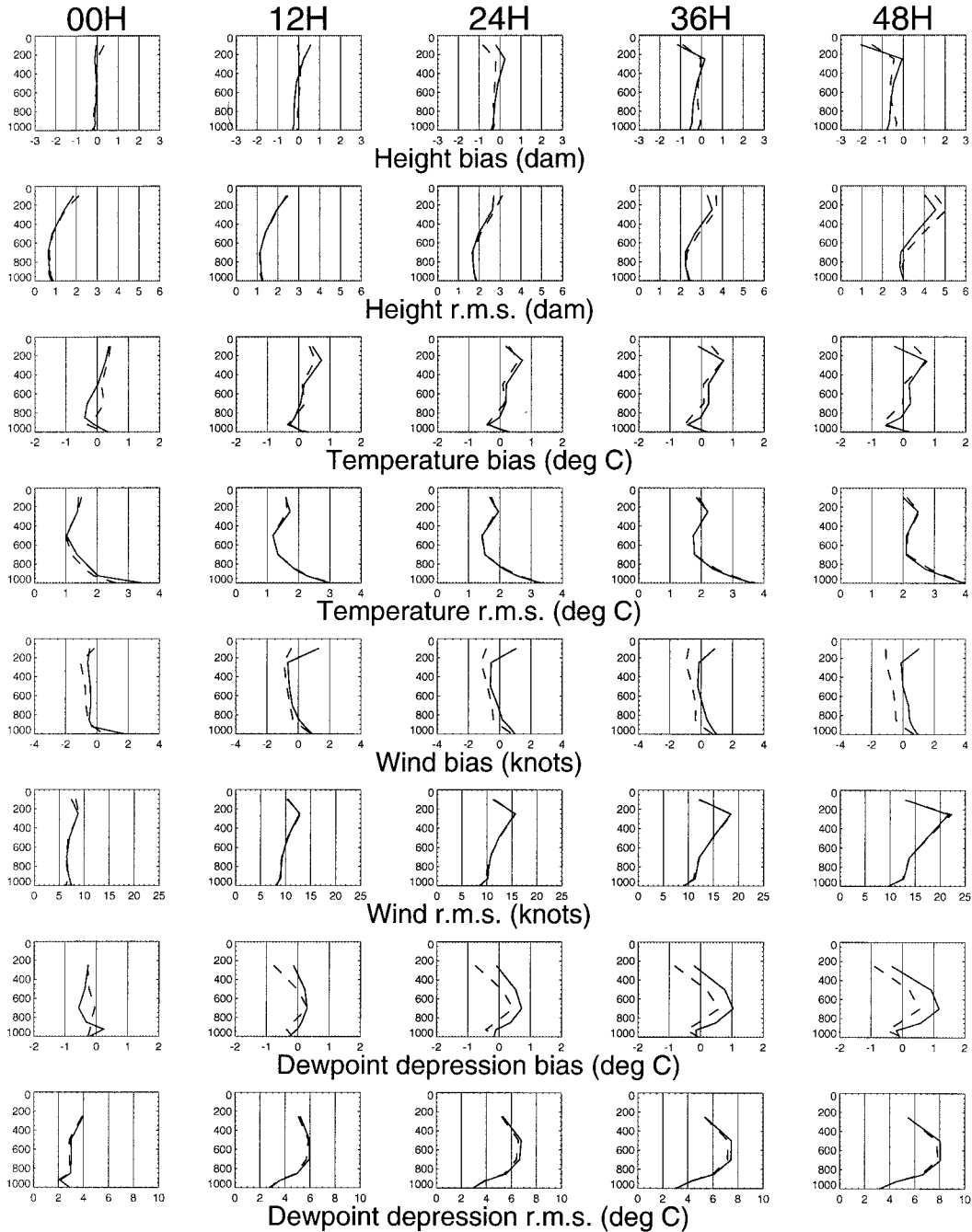


FIG. 10. Bias and rms forecast errors of the RFE and GEM models, as a function of time (going from left to right), and as measured against North American radiosonde soundings (about 120 per verification time). The errors for height (dam), temperature (K), wind (kt), and dewpoint depression (K) are averaged over 163 cases from the period 1 December 1996–26 February 1997. The ordinate for each panel is pressure (hPa).

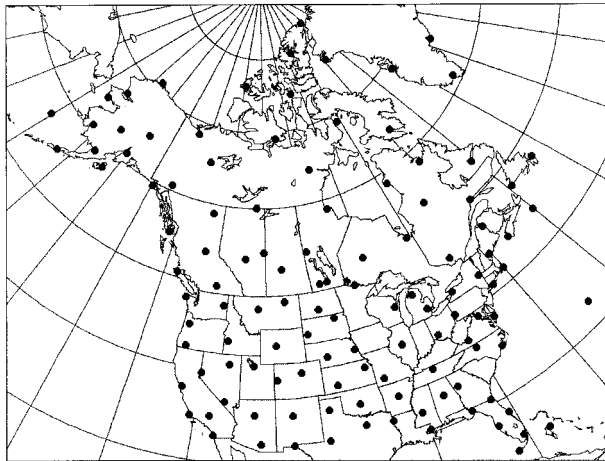


FIG. 11. Typical station distribution for the North American radio-sonde network used for the forecast verification.

mostly on positions and depths of significant weather systems and their associated vertical structures, temperature regimes, upper-level jet streams, boundary layer features, and precipitation forecasts, including both type and amount. During the preimplementation period, the forecast fields for both the RFE and GEM models were output at 3-h intervals to 48 h. This permitted direct comparisons between the model forecasts and the verifying analyses and observations.

The subjective evaluation is first summarized, followed by more detailed comments on points of particular interest to field forecasters. Because of the length (almost three months) of the preimplementation period, we consider the conclusions drawn below to be quite reliable.

#### *a. Summary of the subjective evaluation*

In general, the mass-field forecasts of the GEM and RFE models are very similar. Daily comparative evaluations have, however, revealed some subtle systematic forecast differences that permit a characterization of the relative behavior between the two models. This has led to the conclusion that the GEM model's forecasts are in general slightly better than those of the RFE model. Unless otherwise noted, differences between forecasts increase with forecast time except quite early in the integration, for reasons explained later. For the few instances when the mass-field forecasts of the GEM and RFE models were significantly different, each model's forecast was judged superior to the other's about the same number of times, with no net advantage to either model.

#### *b. Mean sea level pressure, geopotential, and weather systems*

The surface lows forecast by the GEM model are often somewhat deeper than those of the RFE model,

with differences in central pressure of typical surface lows ranging from 2 hPa to as much as 6 hPa deeper, but it should not be inferred that the GEM model systematically develops lows more than the RFE model does. There was a number of cases (including a significant east coast system) where the GEM model developed a low less than the RFE model did, and verified better. For the position and depth of systems, the GEM model's forecasts generally verify a little better than those from the RFE model, albeit by a relatively narrow margin. Deep lows are mostly better forecast by the GEM model than by the RFE model.

It has also been observed that the GEM model often forecasts the upper-air winds to be slightly stronger, and upper-air features to move a little faster, than does the RFE model. In particular, the GEM model forecasts more intense jet streams. This behavior is systematic enough to be quite noticeable in the vertical profiles of the wind displayed in Fig. 10: the winds forecast by the GEM model are on average 1 kt stronger than those forecast by the RFE model. Cold and warm fronts are also propagated slightly faster by the GEM model than by the RFE model, and so of course are the associated troughs. This behavior is consistent with the GEM model forecasting stronger systems and displacing them faster, and is evident in the low-level thickness patterns forecast by both models, with the GEM model verifying better in many situations. The increased phase speeds of the main tropospheric features and the somewhat stronger winds observed in the GEM model forecasts are probably due to the absence of a stratospheric sponge and less horizontal diffusion in the GEM model configuration when compared to that of the RFE model.

During the early part of January, there were periods when significant differences were observed over the western part of the continent in the height and wind fields above 500 hPa, particularly for systems moving in from the edge of, or outside the uniform-resolution window of the RFE model grid. More often than not, these situations were better forecast by the GEM model.

#### *c. Temperature and humidity*

Although the verifications against radiosonde data show (Fig. 10) that the temperature field produced by the GEM model has a slightly stronger positive bias in the middle troposphere than that of the RFE model, this signal was not apparent in the day-to-day comparative evaluation of the model forecasts. Furthermore, although the objective evaluation (see Fig. 10) shows that the GEM model is generally drier than the RFE model, only minor differences for the dewpoint depression, much smaller than those appearing in Fig. 10, have been observed for humid areas associated with weather systems. In dry areas however, the dewpoint depressions forecast by the GEM model are

TABLE 5a. Percentage of explained variance and bias for statistical pointwise temperature forecasts obtained from predictors from the GEM and RFE models, respectively, measured at over 150 stations in Canada for the period 1 December 96 to 5 February 97.

Fore- cast (h)	0000 UTC				1200 UTC			
	GEM		RFE		GEM		RFE	
	Exp. var.	Bias						
6	88.55	-0.10	88.66	-0.17	89.70	-0.11	89.86	-0.16
12	83.60	-0.46	83.51	-0.69	86.38	-0.24	86.42	-0.29
18	82.55	-0.35	82.49	-0.39	81.36	-0.47	81.46	-0.57
24	81.30	-0.47	81.10	-0.50	78.22	-0.68	77.95	-0.78
30	76.44	-0.62	76.69	-0.52	78.61	-0.44	78.22	-0.56
36	74.26	-0.77	73.56	-0.68	77.14	-0.46	76.65	-0.59
42	74.14	-0.43	73.59	-0.36	72.58	-0.62	72.10	-0.77
48	72.97	-0.46	72.28	-0.46	69.04	-0.74	68.09	-0.89

quite often slightly larger than those of the RFE model.

#### d. Precipitation

Since precipitation is one of the most important variables forecast by modern numerical weather prediction models, special attention was given to this field during the evaluation period. A thorough assessment of this highly discontinuous field requires observational data in both quantity and quality that far surpasses that available to the CMC. Moreover, any evaluation suffers from a seasonal dependence since precipitation at midlatitudes exhibits a seasonal cycle: in winter it is primarily associated with major synoptic systems, whereas it is predominantly convectively driven in summer. Although intense convective activity does occur in winter at midlatitudes, it mostly does so over oceanic areas (e.g., over the Gulf Stream) with few verifying observations.

Precipitation forecasts produced by both the GEM and RFE models have been compared among themselves as well as with all the available observations (including radar charts) for various time periods and time ranges. Overall, the GEM model forecasts slightly less precipitation than the RFE model, and this is particularly true for the early (0–6 h) time period. This result is not surprising given the absence of a spinup data assimilation cycle for the GEM model in the preimplementation evaluation. In particular, a spinup cycle allows the precipitation rate to more rapidly achieve realistic values. Depending on the synoptic situation, it takes 6–9 h for the precipitation rates in the GEM model to reach values comparable to those of the RFE model. Thus the 0–12-h accumulated precipitation amounts forecast by the GEM model are generally (but not always) smaller than those forecast by the RFE model, with the differences for the most part being confined to the first 6-h period. The 0–12-h differences can at times reach 15%–20% of the maximum value forecast within a precipitation system, and this typically occurs for events where there is significant convective precipitation.

In general the overall precipitation envelopes (defined here to be the area enclosed by the 1-mm water-equivalent isohyet) forecast by the two models are fairly similar. However those of the GEM model tend often (but not always) to be slightly less extensive than those of the RFE model. There has been a number of cases where the slightly smaller envelope of the GEM model's forecast better fit the available precipitation observations, but there has also been a number of cases where widespread light precipitation resulting in small snow accumulations (i.e., a trace or so) over large areas was better handled by the RFE model.

The precipitation maxima forecast by the GEM model are often lower than those of the RFE model, particularly if convective precipitation is important. Smaller differences occur if purely stratiform precipitation is forecast by both models. For significant precipitation events associated with synoptic developments (particularly if convection is present), both the precipitation maxima and the envelope of the most significant isohyets are often forecast by the RFE model to be larger. Often the RFE model's precipitation forecast has been judged to be marginally better than that of the GEM model, but the difference is generally small unless deep convection is involved. For the latter case, there is generally no indication that the precipitation forecast of either model is superior to that of the other, only that they are different.

For some wintertime synoptic or convective systems that develop over the Gulf Stream or in the northern part of the Gulf of Mexico, the precipitation amounts forecast by the RFE model can be twice as large as those of the GEM model and this difference appears to be greatest for the 36–48-h time period. Although there is very little data to verify these cases, the RFE model's precipitation forecasts look unrealistically high for a quite significant proportion of them, and it is therefore far from clear that this behavior is desirable.

For the few situations that occurred during the evaluation period where several precipitation types were associated with a weather system, the precipitation type diagnosed from the GEM model's vertical tem-

TABLE 5b. Percentage of explained variance for statistical precipitation probability forecasts obtained from predictors from the GEM and RFE models, respectively, measured at over 150 stations in Canada for the period 1 December 1996 to 5 February 1997.

Forecast (h)	0000 UTC		1200 UTC	
	GEM	RFE	GEM	RFE
0-6	34.37	33.45	35.17	34.00
6-12	29.34	27.85	33.26	31.36
12-18	29.24	27.58	28.85	27.46
18-24	30.06	28.73	26.56	24.99
24-30	26.14	24.90	26.75	24.88
30-36	23.67	20.82	26.11	24.47
36-42	22.37	20.67	23.45	22.68
42-48	20.67	19.00	20.16	17.75
0-12	36.05	34.26	37.78	35.44
12-24	32.95	30.42	31.89	29.40
24-36	28.50	25.68	29.76	27.03
36-48	25.18	22.24	25.36	23.81

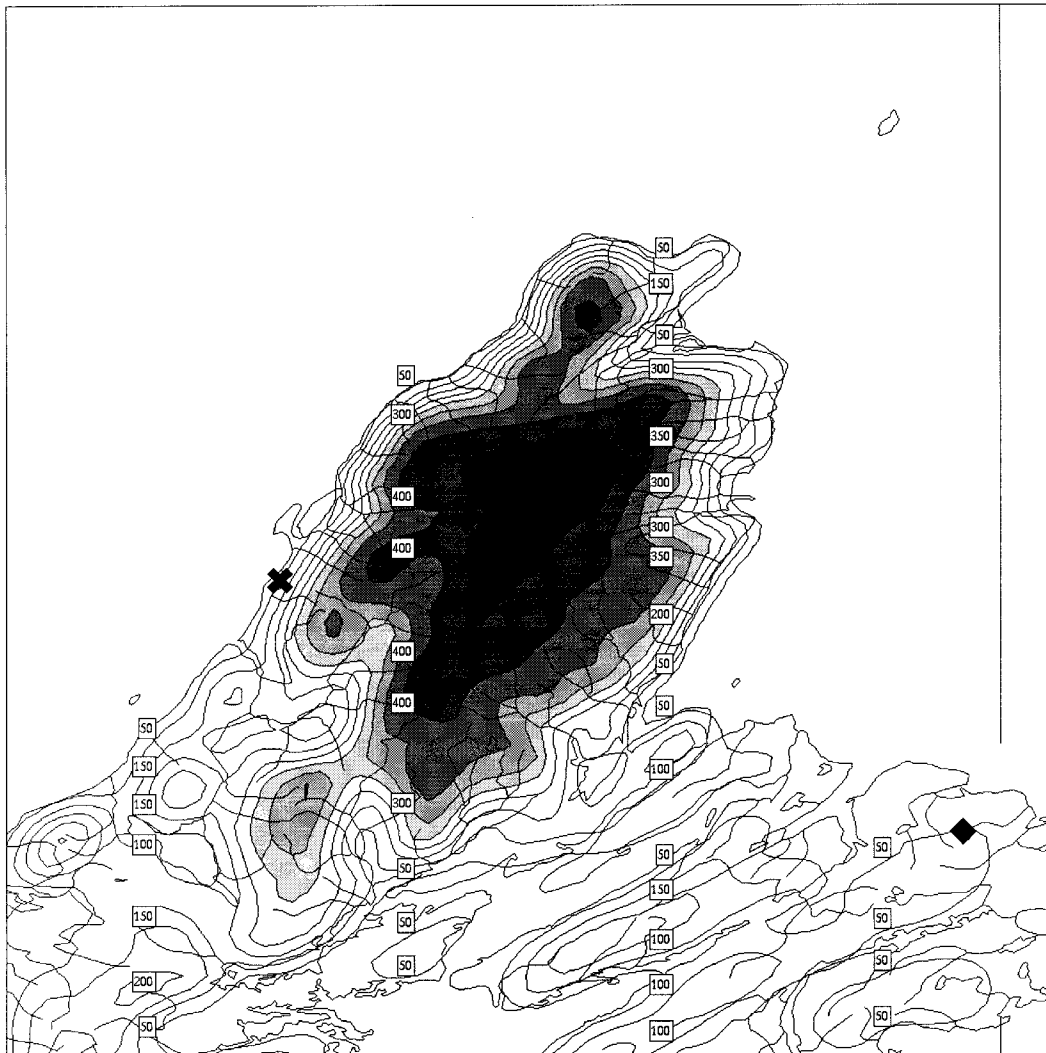


FIG. 12. The GEM model's orography over Cape Breton Highlands at 0.02° resolution. Contour interval is 50 m. Locations of the Grand Étang and Sydney stations are denoted by a thick cross and a diamond, respectively.

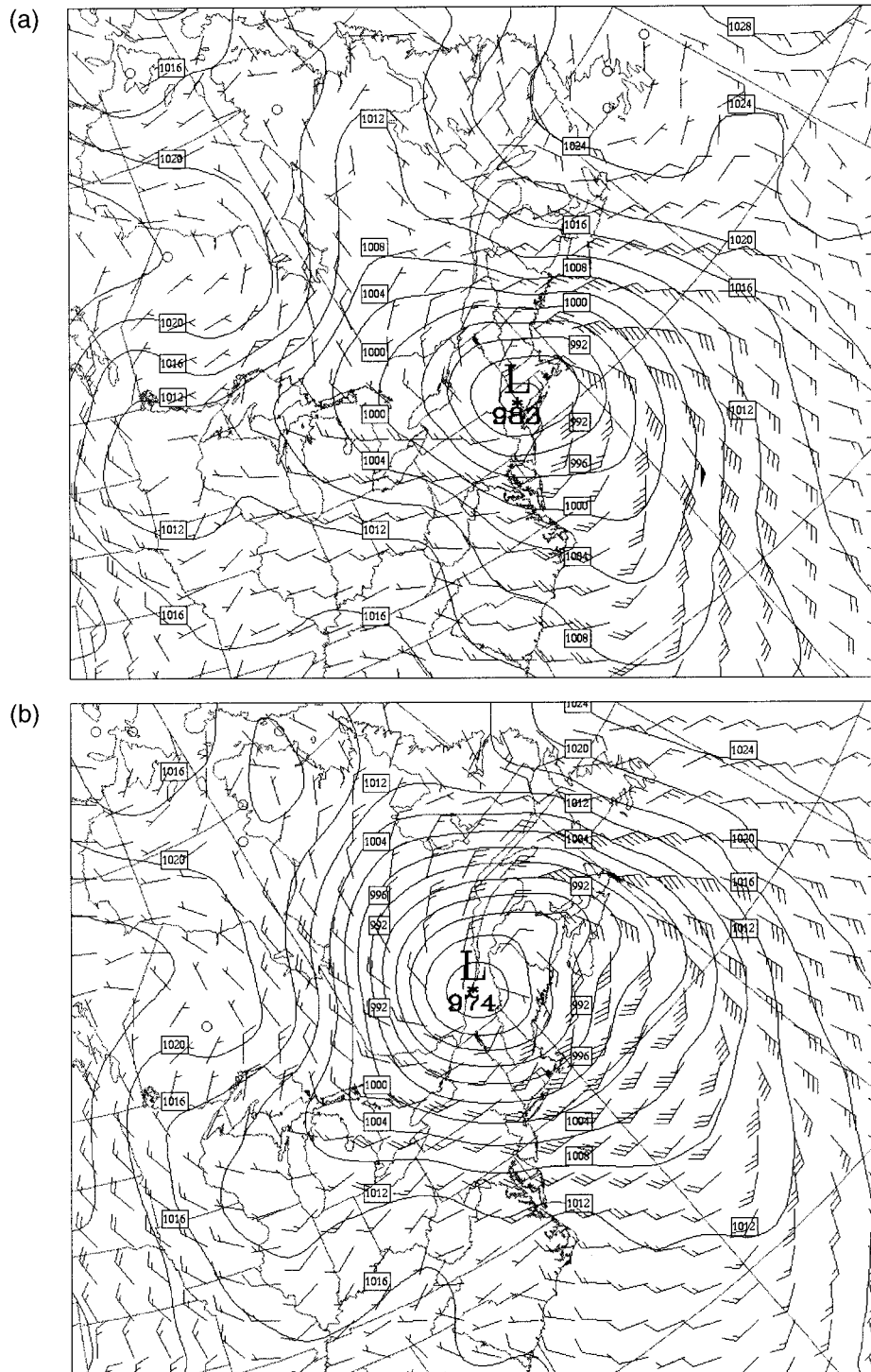


FIG. 13. Mean sea level pressure (contour interval; 4 hPa) and 10-m wind barbs (kt) obtained from CMC analyses at (a) 1800 UTC 21 December 1993 and (b) 0600 UTC 22 December 1993.

perature structure was evaluated as being slightly better than that of the RFE model. The sample of cases is, however, very small, and no definite conclusion can be drawn.

## 6. A meso- $\gamma$ -scale feasibility simulation

The global variable mesh strategy adopted for the GEM model permits a focusing of the resolution much

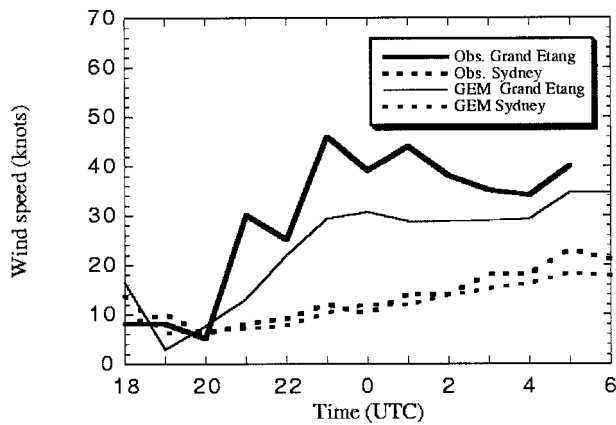


FIG. 14. Observed (heavy) and simulated-by-GEM-model (thin) 10-m wind speeds (kt) from 1800 UTC 21 December 1993 to 0600 UTC 22 December 1993 for the downstream Grand Étang station (solid) and the upstream Sydney station (dashed).

beyond the regional configuration presently used operationally. This potential will enable the model to fulfill future forecasting needs for an ever-increasing resolution of mesoscale phenomena. The strategy also enables the model to be used for hindcasting and for addressing finescale air quality issues.

This section describes a feasibility study performed *not* to provide a detailed and accurate hindcast of a windstorm (an objective that would in any case be very much limited by the paucity of mesoscale initial and verifying data), but rather to concretely demonstrate the numerical feasibility of using a global variable-resolution model for meso- $\gamma$ -scale simulation. A large-scale analysis, as opposed to a mesoscale one, is used for the experiments presented herein. It is found that despite this, the model integrations provide a reasonably realistic mesoscale hindcast. This implicitly means that the response to small-scale orographic forcing is more important for this particular case than is a mesoscale representation of the atmosphere at initial time, that is, the forced response dominates the free response. This will

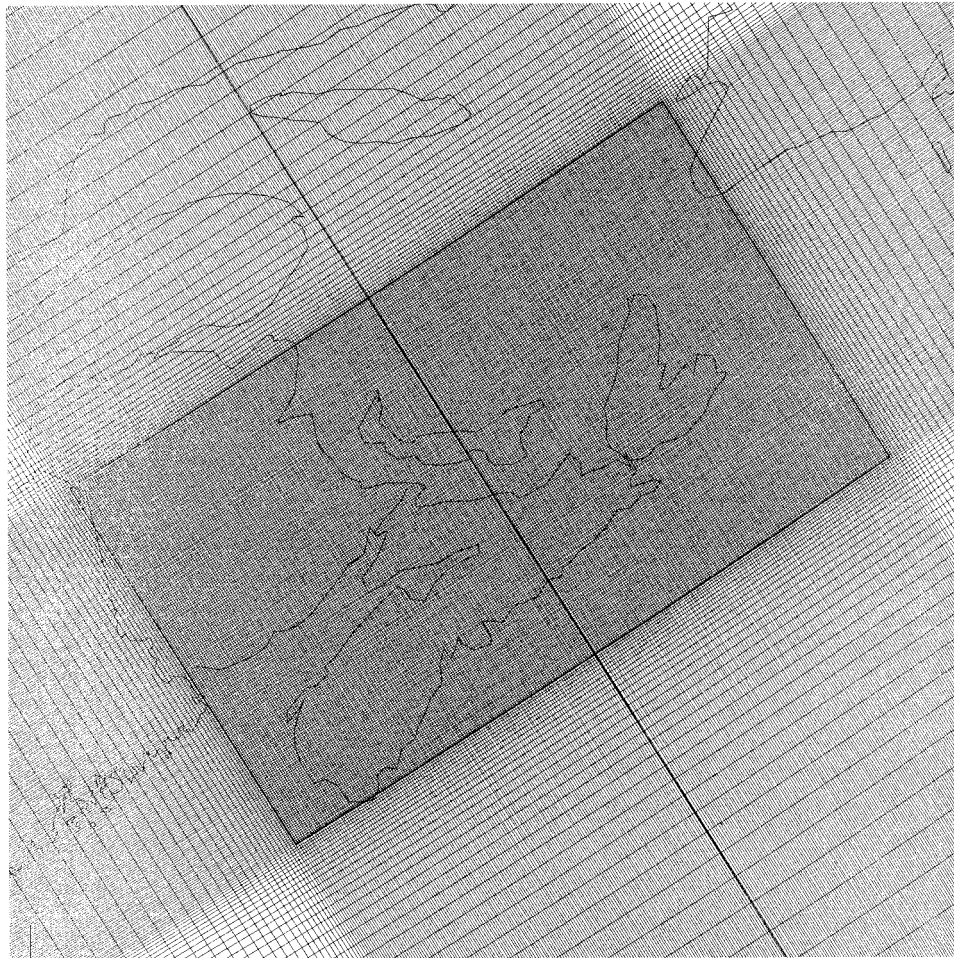


FIG. 15. The  $200 \times 300$  uniform-resolution  $0.02^\circ$  window, centered on  $46^\circ\text{N}$ ,  $63^\circ\text{W}$  of the  $329 \times 418$  global variable-resolution mesh used to simulate the suete.

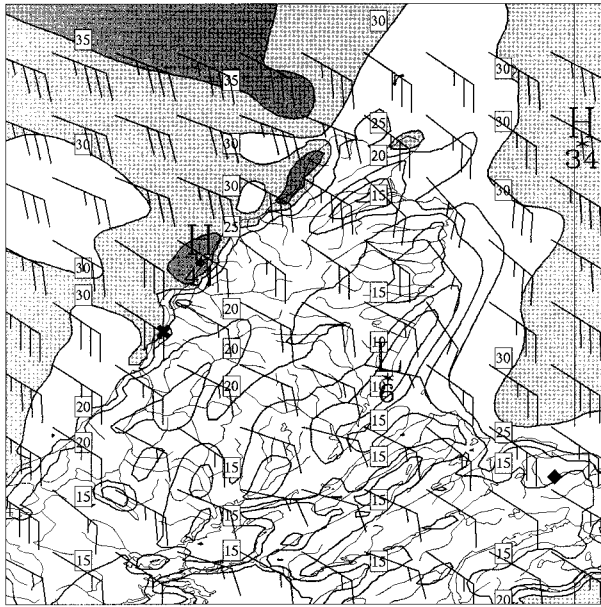


FIG. 16. The 10-m wind speed, valid at 0300 UTC 22 December 1993, as simulated by the GEM model after 9 h of integration; contour interval is 5 kt. Wind barbs (full 10 kt; half 5 kt) are also displayed at every eighth mesh point in each direction. Locations of the Grand Étang and Sydney stations are denoted by a thick cross and a diamond, respectively.

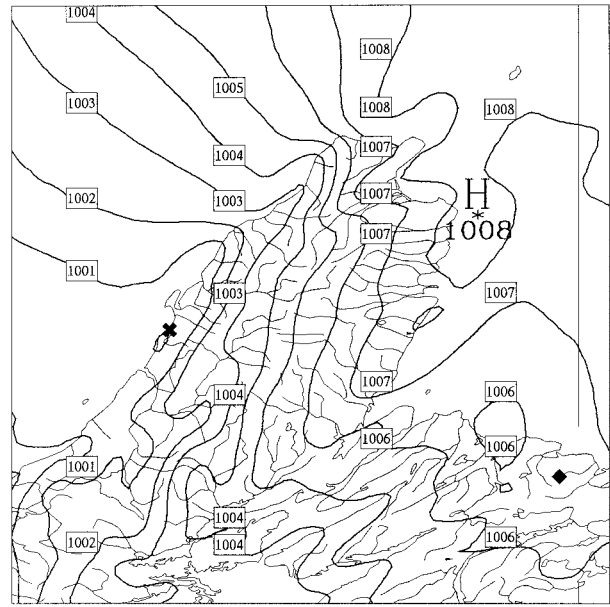


FIG. 17. Mean sea level pressure (hPa), valid at 0300 UTC 22 December 1993, as simulated by the GEM model after 9 h of integration; contour interval is 1 hPa. Locations of the Grand Étang and Sydney airport stations are denoted by a thick cross and diamond, respectively.

not, of course, be true in general. To realistically forecast phenomena such as rainbands or convective complexes will require both mesoscale data to be available and significant advances to be made in mesoscale data assimilation.

The GEM model is integrated to simulate the downslope windstorm (locally termed a “suede”) over the Cape Breton Highlands (see Fig. 12), described in Benoit et al. (1997, hereinafter referred to as B97). This is a particularly appropriate test case for the hydrostatic GEM model since B97 concluded that nonhydrostatic effects for this particular event are relatively unimportant. Their argument is based on a Froude number analysis and a comparison of hydrostatic and nonhydrostatic integrations at 2-km horizontal resolution.

#### a. Synoptic situation

The synoptic situation described in detail in B97 is now briefly summarized. Between 1200 UTC 21 December 1993 and 1200 UTC the following day, an initial 992-hPa surface low pressure system located in the Delaware Bay region moved northeastward to Quebec City and deepened to 973 hPa (see Fig. 16 of B97 for 1200 UTC 21 December 0000 UTC 22 December and 1200 UTC 22 December, and Fig. 13 of the present work for 1800 UTC 21 December and 0600 UTC 22 December). Strong southeasterly winds developed ahead of the warm sector over Nova Scotia

leading to the onset of the downslope suede windstorm observed (see the heavy solid curve of Fig. 14) from 2000 UTC 21 December to approximately 0900 UTC 22 December by the automatic station located at Grand Étang on the western lee side of the Cape Breton Highlands (Fig. 12). A frontal trough swept across Nova Scotia around 0600 UTC 22 December, causing the winds to shift from southeasterly to southwesterly and thereby leading to the breakdown of the suede event during the following few hours. At the upstream Sydney (airport) station (see Fig. 12 for its location), the observed wind intensity (the heavy dashed curve of Fig. 14) is significantly weaker throughout the 24-h period than at the downstream Grand Étang station. Also, the very rapid increase in wind intensity between 2000 and 2300 UTC 21 December observed at Grand Étang is not observed at Sydney.

#### b. Model configuration

In B97 the MC2 (Mesoscale Compressible Community) model and a nested-grid strategy (with three different resolutions, domains, and integration periods, see their Fig. 17) were used to produce a 7-h simulation (between 2100 UTC 21 December and 0400 UTC 22 December) of the suede at 2-km horizontal resolution over a domain of size 340 km × 280 km with 25 vertical levels.

A much simpler single-mesh strategy is employed here to simulate the suede at 0.02° (~2.2 km) hori-

zontal resolution over a three-times-larger ( $6^\circ \times 4^\circ \sim 660 \text{ km} \times 440 \text{ km}$ ) domain with 28 vertical levels (Fig. 1) for almost twice the time period (12 h vs 7 h) starting from the 1800 UTC 21 December analysis (Fig. 13a) and terminating at 0600 UTC 22 December (Fig. 13b). The  $200 \times 300$  uniform-resolution ( $0.02^\circ$ ) window of the  $329 \times 418$  horizontal mesh is displayed in Fig. 15. The principal motivation for choosing to cover a larger area at such a high resolution and integrating for a longer time period than in the B97 study is to better illustrate the point that the global variable-resolution strategy of the GEM model is indeed feasible for simulating very computationally challenging meso- $\gamma$ -scale flows under realistic conditions.

The orientation of the mesh is approximately aligned with the upper-level flow and has sufficient extent to ensure that the embedding synoptic-scale flow is well resolved. This is indeed found to be so with the simulated central pressure of the surface low matching the analyzed values at 0000 and 0600 UTC 22 December. The time step (1 min) is taken to be twice as long as that of the MC2 model's simulation since the GEM model has a two-time-level discretization compared to the three-time-level one of the MC2 model, and therefore both models take time differences over the same interval of time (1 min) and have similar time-truncation errors. The same 28 levels (Fig. 1) of the operational regional configuration of the GEM model are used with exactly the same set of physical parameterizations, except that the gravity wave drag and Kuo convective schemes are turned off, and a simple supersaturation removal scheme is used instead of the Sundqvist parameterization. The orography (Fig. 12) and land-sea mask are obtained from an available high-resolution database, but the surface roughness length had to be interpolated from the  $0.33^\circ$  resolution operational field. The diffusion coefficient for the present simulation is taken to be  $2500 \text{ m}^2 \text{ s}^{-1}$  for all prognostic variables. This is comparable to the value of  $1920 \text{ m}^2 \text{ s}^{-1}$  used at 10% higher horizontal resolution in B97 for all prognostic variables except vertical momentum, for which a five-times-larger value was employed.

### c. The simulation

The 10-m wind speed and MSLP fields over the Cape Breton Highlands, simulated by the GEM model and valid at 0300 UTC 22 December, are displayed in Figs. 16 and 17, respectively. They are quite similar to the corresponding fields of the B97 integrations (their Figs. 24 and 20). The incident southeasterly flow coming in from the ocean is altered by the mesoscale reorganization of the circulation over and around Cape Breton, and slowed down by both the enhanced surface drag over the highlands and the upward slope of the orography to its crest. The flow then

sharply accelerates over the very steep downward slope on the lee side of this crest to produce two strong and narrow near-surface jets (Fig. 16), with wind intensities greater than 35 kt and a maximum intensity of 41 kt. These areas of high wind speed are located just offshore and in the northwestern lee of the highlands, and are aligned parallel to the coast.

A mesoscale pressure trough (Fig. 17) has developed along the coast on the northwestern lee side of the mountain crest with an associated mesoscale ridge on the windward side. The simulation also gives a strong mesoscale sea level drop in pressure across the highlands of approximately 7 hPa over a horizontal distance of approximately 75 km. Fortuitously, the maximum and minimum simulated pressures occur fairly close to the upstream Sydney and downstream Grand Étang observing stations, respectively. The simulated and observed pressure differences between these two stations at 0300 UTC December 22 are 6.3 and 8.3 hPa, respectively, giving credence to the simulation.

The latitude and longitude of the locations of these two observing stations as defined in the World Meteorological Organization Station Dictionary (WMO 1998) is only given to the nearest minute of arc ( $\sim 2 \text{ km}$ ). This means that the station locations could in reality be anywhere within a radius of approximately 1 km (about half the mesh length) or so of that defined by the station dictionary, causing a sampling problem. For the MSLP field this is not at all serious since sampling the field a half mesh length away from that defined by the dictionary negligibly perturbs the results due to the relative smoothness of this field in the vicinity of the stations. For the wind speed field the problem is more serious. Shifting the station location by a half mesh length at the Grand Étang station can, for example, change the sampled simulated result at 0300 UTC 22 December by plus or minus 4 kt, due to the very large gradient of this field at this station in the direction normal to the coast. Also, the finite resolution of the mesh inherently smooths the orography, and this is likely to have a nonnegligible quantitative effect on the flow.

Nevertheless, it is still useful to qualitatively compare the simulated 10-m wind speed at the stations with that observed. It can be seen from Fig. 14 that the rapid onset of the downslope windstorm at Grand Étang between 2000 and 2300 UTC 21 December is qualitatively well simulated, while no abrupt increase in wind speed occurs at the upstream Sydney station. Quantitatively, the agreement is excellent at the upstream station, for which the sampling of the wind speed is insensitive to a displacement of a half mesh length. For the downstream Grand Étang station, the wind speed is generally somewhat underestimated. This is not surprising given the above-described sampling error and the limitations of the experiment; for example, the absence of a mesoscale analysis, the use

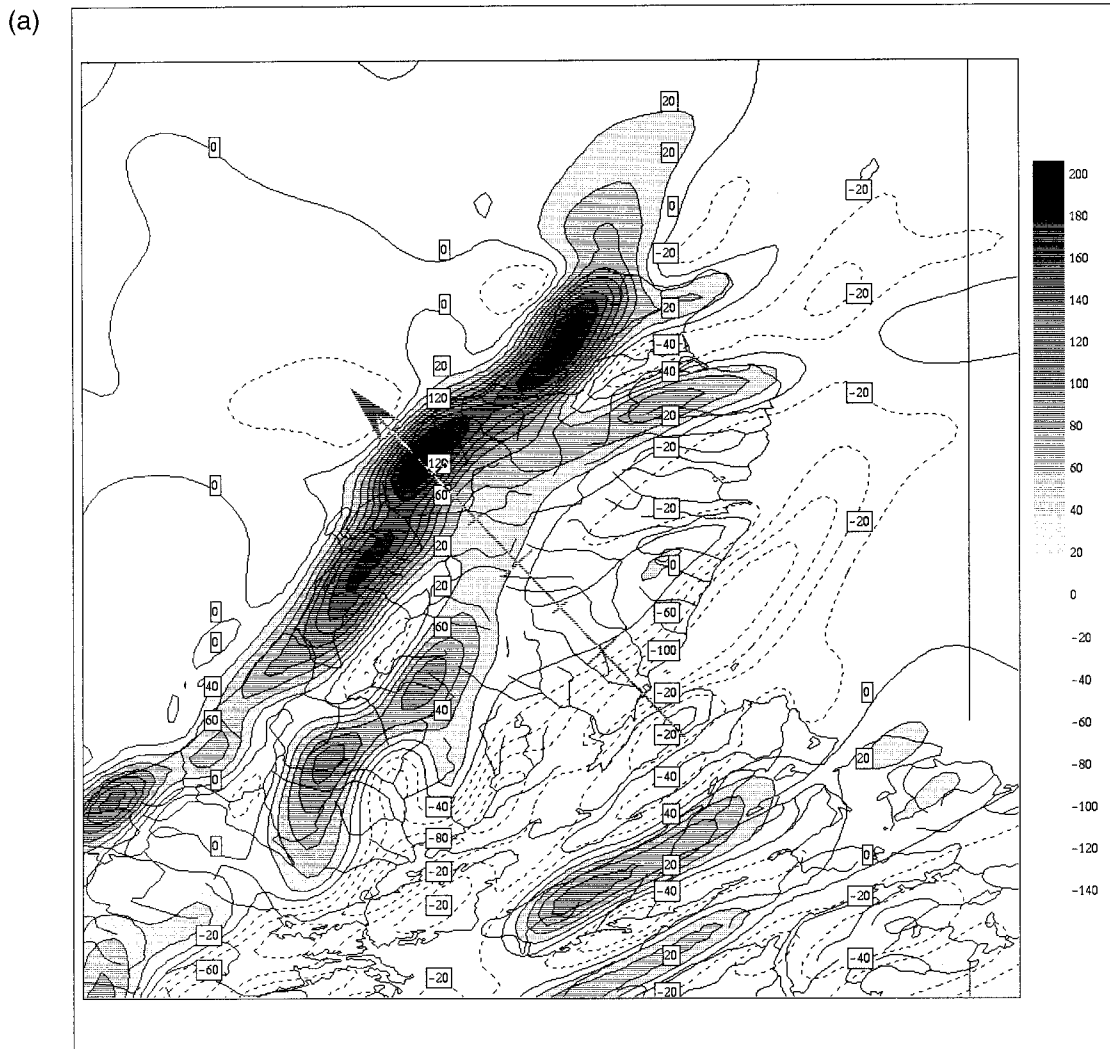


FIG. 18. Nine-hour forecast of vertical motion ( $\omega \equiv dp/dt$ ), valid at 0300 UTC December 22 1993 (a) at 900 hPa, contoured every  $2 \text{ Pa s}^{-1}$  ( $\equiv 20 \times 10^{-1} \text{ Pa s}^{-1}$ ); (b) a vertical cross section along baseline drawn on (a) with terrain silhouette, contoured every  $2 \text{ Pa s}^{-1}$  ( $\equiv 20 \times 10^{-1} \text{ Pa s}^{-1}$ ).

of a too-smooth definition of roughness length, and the limited resolution.

The results displayed in Fig. 21 of B97 for the MC2 model with 2-km resolution can be compared to those shown in Fig. 14 of the present work for the GEM model at similar resolution. At the upstream Sydney station, the MC2 model's 2-km-resolution integration significantly overestimates the intensity of the 10-m wind speeds (their Fig. 21b). The simulated values are about twice as large as the observed sustained wind speed (i.e., the average value within a grid box that a model represents), and significantly larger even than the observed gusts. On the other hand, the GEM simulation gives an excellent estimate of the sustained wind speed.

For the downstream Grand Étang station, the sit-

uation is somewhat different: the winds from the MC2 model's simulation exceed the sustained wind speed, but are below the observed gusts (their Fig. 21a). As for the GEM model's simulation (Fig. 14a), except for the first 2 h of integration, the winds are weaker than those of the sustained wind observations.

Horizontal and vertical cross sections of the vertical velocity ( $\omega \equiv dp/dt$ ), valid at 0300 UTC 22 December 1993, are displayed in Fig. 18. These may be compared with the corresponding plots given in Figs. 22a,b and 23a,b of B97 for the nonhydrostatic and hydrostatic integrations of the MC2 model, respectively, at 2-km resolution. The qualitative agreement between the three integrations is quite good and even the quantitative agreement is generally good. For example, the upstream vertical tilts of the vertical cross

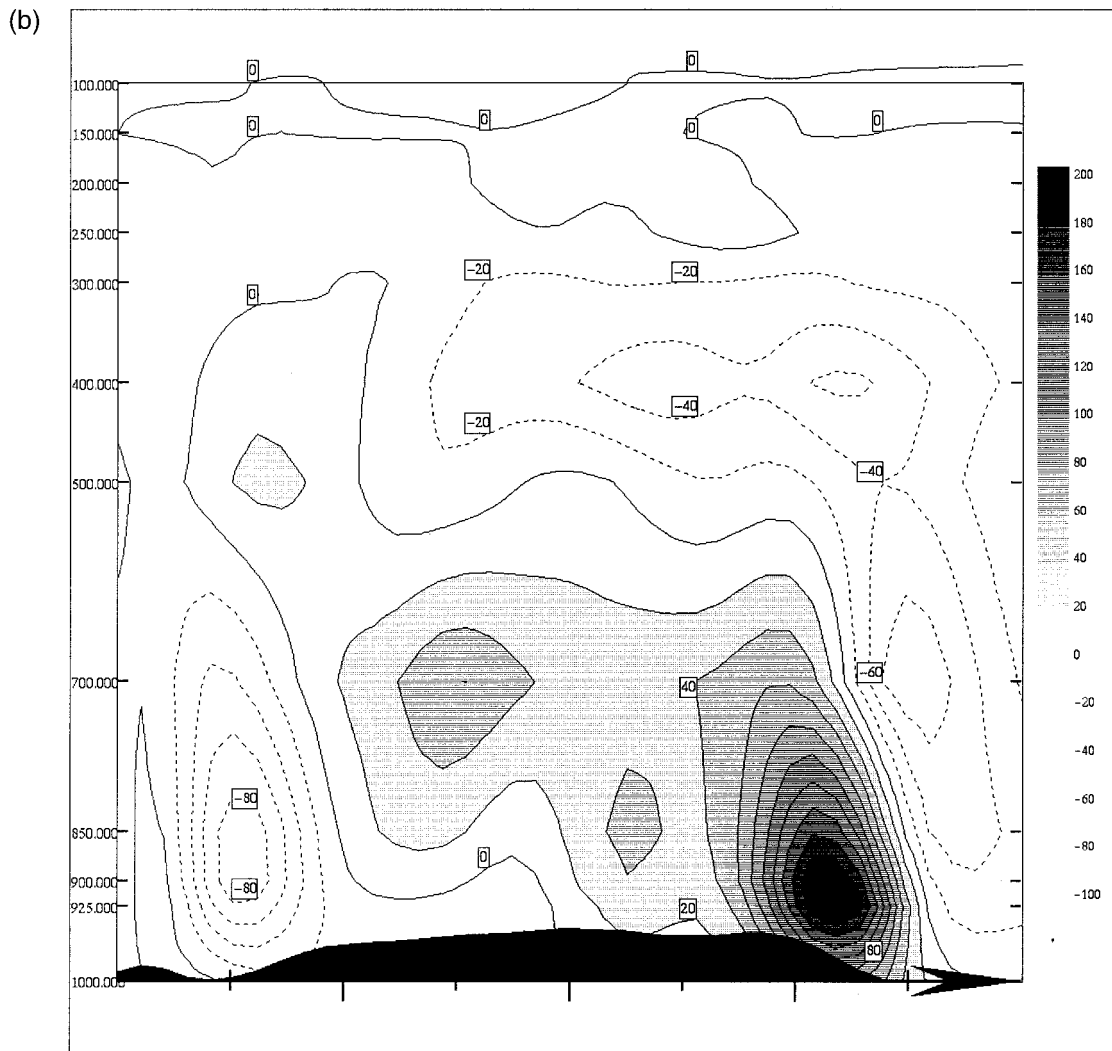


FIG. 18. (Continued)

section of the vertical velocity of the two hydrostatic integrations (Fig. 18b of the present paper and Fig. 23b of B97) are very similar, and the values for the associated low-level subsidence and ascent are quantitatively also very similar.

From the above discussion, it is concluded that the two simulations are of comparable quality, and that it is possible to perform meso- $\gamma$ -scale simulations with a global variable mesh. For improved physical validity however, it is recognized that the model should employ the nonhydrostatic Euler equations as governing equations, together with appropriate parameterizations of any unrepresented physical processes.

### 7. Conclusions

A variable-resolution Global Environmental Multi-scale (GEM) model has been constructed based on the

strategy and model formulation described in Part I of this two-part paper. Experiments confirm the potential of the proposed strategy for a broad range of scales.

Medium-range integrations of the GEM model have been run daily over a nine-month period with uniform horizontal resolution almost identical to that of CMC's operational spectral SEF model. For the model configurations of the comparison, it was found that the GEM model performed somewhat better than the operational SEF model.

For regional forecasting at the continental scale, a controlled set of experiments shows that differences between the 48-h forecasts for the 500-hPa geopotential height and MSLP fields obtained from a uniform horizontal resolution integration, and those obtained from a variable-mesh one with equivalent resolution over a North American window, are acceptably small. A meso- $\gamma$ -scale simulation shows the ability of the global variable-resolution mesh strategy to address the trend in

forecasting needs for ever-finer resolution of mesoscale features. It also demonstrates the GEM model's potential as a simulation tool for hindcasting and for addressing finescale air quality issues. After almost three months of comparative tests performed under operational conditions, on 24 February 1997 the GEM model replaced CMC's formerly operational Regional Finite Element model. It is now run twice daily to provide 48-h weather forecasts over North America.

*Acknowledgments.* Many people from the Canadian Meteorological Centre and the Meteorological Research Branch contributed to the recent operational implementation at the CMC of the GEM model, including many who also contributed to the development phase. The authors are grateful to the staff of CMC's Implementation and Operational Services Division for implementing the model in a parallel evaluation run and then operationally, and to the CMC operational meteorologists for their contributions to the evaluation of the new model's meteorological performance.

Among those not already mentioned at the end of Part I, particular thanks are due to Michel Baltazar, Bernard Bilodeau, Normand Brunet, Gérard Croteau, Louise Faust, Michel Grenier, Patrick Hertel, Richard Hogue, André Plante, and Richard Verret for the technical support they afforded during the project's operational phase.

#### REFERENCES

- Benoit, R., M. Desgagné, P. Pellerin, S. Pellerin, Y. Chartier, and S. Desjardins, 1997: The Canadian MC2: A semi-Lagrangian, semi-implicit wideband atmospheric model suited for finescale process studies and simulation. *Mon. Wea. Rev.*, **125**, 2382–2415.
- Chouinard, C., J. Mailhot, H. L. Mitchell, A. Staniforth, and R. Hogue, 1994: The Canadian regional data assimilation system: Operational and research applications. *Mon. Wea. Rev.*, **122**, 1306–1325.
- Côté, J., M. Roch, A. Staniforth, and L. Fillion, 1993: A variable-resolution semi-Lagrangian finite-element global model of the shallow-water equations. *Mon. Wea. Rev.*, **121**, 231–243.
- , S. Gravel, A. Méthot, A. Patoine, M. Roch, and A. Staniforth, 1997: Preliminary results from a dry global variable-resolution primitive equations model. *The André J. Robert Memorial Volume*, C. Lin, R. Laprise, H. Ritchie, Eds., Canadian Meteorological and Oceanographic Society, 245–259.
- , —, —, —, —, and —, 1998: The operational CMC-MRB Global Environmental Multiscale (GEM) model: Part I. Design considerations and formulation. *Mon. Wea. Rev.*, **126**, 1373–1395.
- Fillion, L., H. L. Mitchell, H. Ritchie, and A. Staniforth, 1995: The impact of a digital filter finalization technique in a global data assimilation system. *Tellus*, **47A**, 304–323.
- Mailhot, J., R. Sarrazin, B. Bilodeau, N. Brunet, and G. Pellerin, 1997: Development of the 35-km version of the operational regional forecast system. *Atmos.–Ocean*, **35**, 1–28.
- , —, —, —, A. Méthot, G. Pellerin, C. Chouinard, L. Garand, C. Girard, and R. Hogue, 1995: Changes to the Canadian regional forecast system: description and evaluation of the 50-km version. *Atmos.–Ocean*, **33**, 55–80.
- Mitchell, H. L., C. Chouinard, C. Charette, R. Hogue, and S. J. Lambert, 1996: Impact of a revised analysis algorithm on an operational data assimilation system. *Mon. Wea. Rev.*, **124**, 1243–1255.
- Rabier, F., A. McNally, E. Andersson, P. Courtier, P. Uden, J. Eyre, A. Hollingsworth, and F. Bouttier, 1998: The ECMWF implementation of three dimensional variational (3D-Var). Part II: Structure functions. *Quart. J. Roy. Meteor. Soc.*, in press.
- Ritchie, H., and C. Beaudoin, 1994: Approximations and sensitivity experiments with a baroclinic semi-Lagrangian spectral model. *Mon. Wea. Rev.*, **122**, 2391–2399.
- Staniforth, A., 1997: Regional modeling: A theoretical discussion. *Meteor. Atmos. Phys.*, **63**, 15–29.
- Verret, R., 1987: Development of a “perfect prog” system to forecast probability of precipitation and sky cover. CMC Tech. Doc. 29, 28 pp. [Available from the Canadian Meteorological Center, Dorval, PQ H9P 1J3, Canada.]
- WMO, 1998: Weather reporting. WMO Publ. 9, Vol. A. [Available from WMO, Case Postale 2300, CH-1211 Geneva 2, Switzerland; or online from <http://www.wmo.ch/web/ddbs/publicat.html>.]